Protons in the near-lunar wake observed by the Sub-keV Atom Reflection Analyzer on board Chandrayaan-1

Y. Futaana,[1] S. Barabash,[1] M. Wieser,[1] M. Holmström,[1] A. Bhardwaj,[2] M. B. Dhanya,[2] R. Sridharan,[2] P. Wurz,[3] A. Schaufelberger,[3] and K. Asamura[4]

Received 7 January 2010; revised 7 July 2010; accepted 12 July 2010; published 29 October 2010.

[1] Significant proton fluxes were detected in the near-wake region of the Moon by an ion mass spectrometer on board Chandrayaan-1. The energy of these nightside protons is slightly higher than the energy of the solar wind protons. The protons are detected close to the lunar equatorial plane at a 140° solar zenith angle, that is, ~50° behind the terminator at a height of 100 km. The protons come from just above the local horizon and move along the magnetic field in the solar wind reference frame. We compare the observed proton flux with the predictions from analytical models of an electrostatic plasma expansion into a vacuum. The observed velocity is higher by a factor of 2 to 3 than the velocity predicted by analytical models. The simple analytical models cannot explain the observed ion dynamics along the magnetic field in the vicinity of the Moon.

Citation: Futaana, Y., S. Barabash, M. Wieser, M. Holmström, A. Bhardwaj, M. B. Dhanya, R. Sridharan, P. Wurz, A. Schaufelberger, and K. Asamura (2010), Protons in the near-lunar wake observed by the Sub-keV Atom Reflection Analyzer on board Chandrayaan-1, *J. Geophys. Res.*, *115*, A10248, doi:10.1029/2010JA015264.

1. Introduction

[2] The classical picture of the Moon-solar wind interaction is straightforward. Because the surface of the Moon is covered by nonconductive porous regolith, it behaves as a perfect absorber of solar wind ions and electrons. The perturbations of lunar origin in the interplanetary magnetic field (IMF) are extremely small, and therefore no significant effects are expected in the upstream solar wind. For example, no global-scale bow shock is predicted and, consistently, has never been observed. Only strongly, but locally, magnetized regions of crustal origin (often called magnetic anomalies) can interact with the solar wind under specific configurations, forming minimagnetospheres [e.g., *Russell and Lichtenstein*, 1975; *Lin et al.*, 1998; *Wieser et al.*, 2010].

[3] Because supersonic solar wind plasma is largely absorbed by the dayside surface, a vacuum region is formed on the nightside of the Moon. Solar wind plasma refills the vacuum region, and corresponding ion signatures were observed during the wake crossings by the Wind spacecraft in 1994 [*Ogilvie et al.*, 1996]. One conclusion from these observations was that a large electric potential drop, of ~400 V, close to the wake boundary has to be assumed to explain the ion signatures. Following the observations by Wind, observations of electrons and protons in the vicinity of the Moon from other missions also suggest that a significant electric potential drop does exist across the boundary [e.g., *Futaana et al.*, 2001; *Halekas et al.*, 2005; *Nishino et al.*, 2009a]. A number of numerical simulations using particle-in-cell models and hybrid models of solar wind-Moon interactions have been performed [*Farrell et al.*, 1998; *Birch and Chapman*, 2001; *Kallio*, 2005; *Trávníček et al.*, 2005], but the large potential drop has not been reproduced. *Halekas et al.* [2005] proposed a theory to explain the large potential drop by considering supra-thermal solar wind electrons.

[4] Apart from the fluid considerations for plasma in the vicinity of the Moon, kinetic effects have also been discussed. Using Apollo observations, *Freeman* [1972] found fluxes of light ions with a mass per charge of less than 10 amu/q from the zenith direction in the deep wake, but the source of these light ions was not clear. *Futaana et al.* [2003] reported nonsolar wind protons with ring-like velocity distribution functions during a lunar swing-by of the Nozomi spacecraft. They interpreted that those protons are probably reflected from a local bow shock formed in front of the lunar minimagnetosphere, but *Holmström et al.* [2010] argued that the reflected protons from the lunar surface discovered by *Saito et al.* [2008] may also explain the Nozomi observations.

[5] In this paper we report on the detection of a proton flux in the deep lunar wake region by the Sub-keV Atom Reflection Analyzer (SARA) on board Chandrayaan-1. Earlier, *Nishino et al.* [2009a, 2009b] identified two types of

[1]Swedish Institute of Space Physics, Kiruna, Sweden.
[2]Space Physics Laboratory, Vikram Sarabhai Space Center, Trivandrum, India.
[3]Physikalisches Institut, University of Bern, Bern, Switzerland.
[4]Institute of Space and Astronautical Science, Sagamihara, Japan.

0148-0227/10/2010JA015264

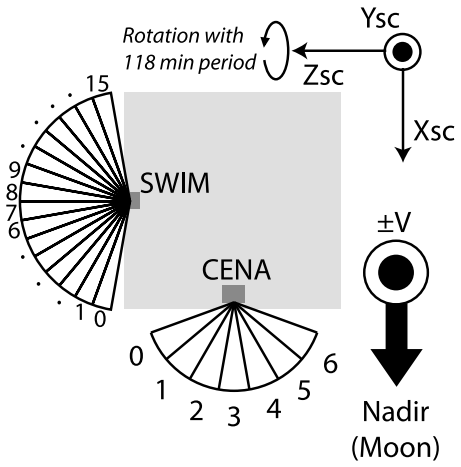

Figure 1. Chandrayaan-1 Energetic Neutrals Analyzer (CENA) and Solar Wind Monitor (SWIM) apertures and the numbering of the viewing directions relative to the spacecraft (sc) reference frame. The SWIM has an ~7 × 160° aperture divided into 16 viewing directions. The CENA aperture is 10 × 160°, divided into seven azimuthal channels. In the nominal nadir pointing the spacecraft velocity is parallel to the $+y_{sc}$ or $-y_{sc}$ axis, and the $+x_{sc}$ axis points to the lunar center.

proton intrusions into the wake in the ion data obtained from the Kaguya spacecraft. However, the arrival direction of proton fluxes reported in this paper is significantly different from the fluxes reported by *Nishino et al.* [2009a, 2009b]. The proton population discussed here is frequently seen in the SARA data, however, we selected one particular event on 25 January 2009 when the IMF and upstream condition were stable and optimal for observations, such that the IMF vector was in the ecliptic plane and perpendicular to the solar wind velocity vector.

2. Instrumentation

[6] The SARA data discussed in this paper were collected on a lunar polar orbit at a height of ~100 km. SARA is composed of two sensors [*Bhardwaj et al.*, 2005; *Barabash et al.*, 2009]. One of the sensors is called the Chandrayaan-1 Energetic Neutrals Analyzer (CENA), which is the first-ever energetic neutral atom sensor flown to the Moon. The other sensor is the Solar Wind Monitor (SWIM), an ion mass analyzer to monitor the solar wind and to study the ion environment around the Moon. Only data obtained by the SWIM sensor are used in this study.

[7] The SWIM sensor is a compact electrostatic ion mass analyzer with a fan-shaped aperture (~7° × 160°) and an angular resolution of ~7° × 10° (depending on the looking direction). The number of angular pixels is 16 (maximum). For this study SWIM was operated in the energy range of ~100 to 3000 eV/q covered by 16 logarithmically separated energy-per-charge bins. The SWIM also has a moderate mass resolution of $m/\Delta m \sim 2$ [*McCann et al.*, 2007; *Barabash et al.*, 2009].

[8] Figure 1 shows the SWIM and CENA fields of view (FoVs). The SWIM bore sight is along the $+z_{sc}$ axis, and the aperture plane is perpendicular to the y_{sc} axis. Here the subscript sc denotes the spacecraft reference frame. The nominal spacecraft attitude is the nadir pointing. During nadir pointing the $+x_{sc}$ axis always points toward the lunar surface. The velocity vector of the spacecraft is nominally along either the $+y_{sc}$ or the $-y_{sc}$ axis. During the period of observation discussed in this paper the $-y_{sc}$ axis was coaligned with the velocity vector. As shown in Figure 1 the SWIM aperture is perpendicular to the spacecraft velocity vector, and some of the SWIM angular sensors

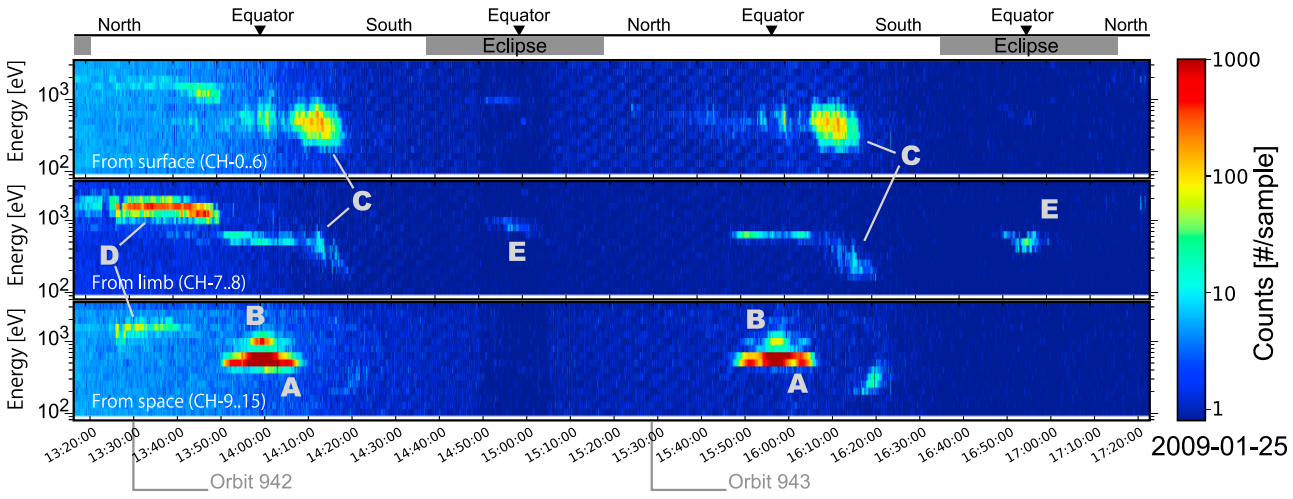

Figure 2. Energy-time spectrograms observed on 25 January 2009 over two consecutive orbits, 942 and 943. (top) The energy-time diagrams for the observed ion counts coming from the surface (below the local horizon), (middle) limb (toward the horizon), and (bottom) space (above the horizon) are shown. At the top the time intervals when the spacecraft was in the lunar shadow (eclipse) as well as the equator crossings are indicated. The spacecraft location (Northern or Southern Hemisphere) is also indicated. Five distinct ion populations are identified, labeled A through E.

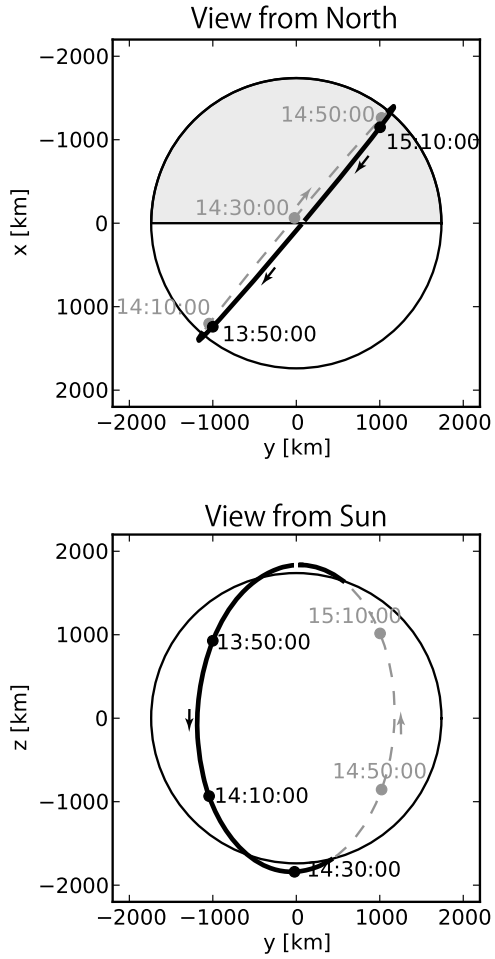

Figure 3. Chandrayaan-1 orbit in the lunar-centric solar ecliptic (LSE) coordinate system (the $+x$ axis is the Moon-Sun line, the $+y$ axis is the velocity vector of the Sun motion relative to the Moon, and the $+z$ axis completes the right-handed system) between 1330 and 1528 UT on 25 January 2009. The orbital period was ~118 min.

(CH-0 to -5) point toward the lunar surface. This configuration means that Chandrayaan-1 can be considered a spinning satellite revolving around the z_{sc} axis with a rotation period equal to the spacecraft orbit around the Moon (~118 min). The SWIM FoV plane (the half-plane of $\pm x_{sc}$ and $+z_{sc}$) can cover an $\sim 2\pi$ angular space (half-hemisphere) in half of the orbital period (~59 min). The three-dimensional (3D) velocity distribution function of the solar wind can be measured only when the spacecraft is at the dayside and the SWIM FoV is close to the ecliptic plane. Therefore, the solar wind can be observed only once per orbit when the spacecraft is close to the lunar dayside equator. The 3D velocity distribution of the protons allows us to calculate the density. We calculated the density of the protons by numerical integration over the observed flux.

[9] In this paper the lunar-centric solar ecliptic (LSE) coordinate system is used. The Moon-Sun line is the $+x$ axis, the velocity vector of the Sun motion relative to the Moon is the $+y$ axis, and the $+z$ axis completes the right-handed system. Indeed, the difference in the axis directions with the geocentric solar ecliptic (GSE) frame ($+x$ axis is the Earth-Sun line, $+z$ axis is normal to the mean ecliptic plane of the Earth pointing to north, and $+y$ axis completes the right-handed system) is in general very small (<0.3°); it was ~0.18° for the day of the observation.

3. Observation

[10] Figure 2 shows the energy-time spectrogram of ion counts observed by the SWIM on 25 January 2009. The lunar phase was 2 days before the new Moon. Because the Moon was in the undisturbed solar wind, no effects from the Earth's bow shock or magnetosphere were expected. Figure 3 shows the Chandrayaan-1 orbit corresponding to the SWIM observations discussed here (orbit 942). The motion of the spacecraft was from north to south on the dayside and from south to north on the nightside. The Sun aspect angle, the angle between the spacecraft orbital plane and the Sun-Moon line, was ~40°.

[11] In the SWIM data shown in Figure 2, five distinct populations of ions, labeled A-E, can be clearly identified. The strongest flux is from the solar wind protons with an energy of ~500–600 eV/q (population A). The corresponding solar wind velocity is ~310–340 km/s. At the same time we can see population B in a slightly higher energy range ($E/q \sim 1$ keV/q) that consists of the α particles from the solar wind. Because the α particles are doubly charged, the actual energy is ~2 keV, and the velocity was similar to that of the solar wind protons (A). These two populations are observed on the lunar dayside close to the lunar equator from directions 11 and 12, as expected.

[12] Ion populations C and D are also detected on the dayside. Both populations are composed of protons as established by mass analysis (not shown here). Population C comes from the surface and has a broadened energy spectrum. These ions are backscattered protons from the lunar surface similar to the observations reported by *Saito et al.* [2008]. Ions of population D are the backscattered protons accelerated by the convection electric field of the ambient solar wind electric field, which was also suggested by *Saito et al.* [2008]. Note that the accelerated protons (D) are absent on the second orbit. The signatures of this population are discussed in section 4.

[13] Population E is a faint proton flux that can be seen in the deep nightside region. The energy of population E is 0.5 to 1 keV, which is slightly higher than that of the solar wind. The densities of solar wind A and population E can be calculated by the integration of the observed flux. The density is 1.7 cm^{-3} for solar wind A and (3–4) × 10^{-3} cm^{-3} for population E. Notably, the density calculation is not straightforward, especially for the case of low ion flux, and therefore a large ambiguity may be included. In addition, the solar wind density is an underestimation because anomalously lower efficiencies than the ground calibration were found in the solar wind channels of the sensor. This is consistent with the solar wind density of 6–8/cm^3 obtained from the Wind/Solar Wind Experiment (SWE) instrument during this period. In contrast, no such lower efficiencies were found in the channels including population E. The density ratio between the nightside ions and the solar wind is then (0.5–2) × 10^{-3}. As mentioned in the Instrumentation section, the SWIM can measure 3D distribution functions

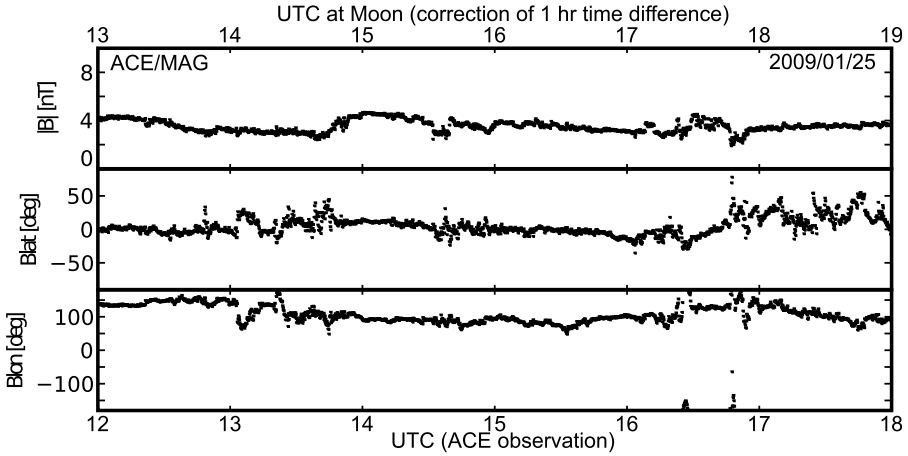

Figure 4. Interplanetary magnetic field (IMF) data observed by ACE between 12–18 UT on 25 January 2009. Considering the propagation time of 1 h from Advanced Composition Explorer (ACE) to the Moon, the solar wind at the Moon corresponds to 1300–1900 UT (upper axis). (top) The magnitude, (middle) latitudinal component, and (bottom) longitudinal component in the geocentric solar ecliptic (GSE) frame of the magnetic field are displayed.

with the help of the spacecraft motion and its pointing. In addition, because ion populations A and E are both narrow beams, with thermal extents of ~10° (full width at half-maximum), as estimated from the velocity spread, almost all of these beams can even be measured at a specific time.

[14] Advanced Composition Explorer (ACE) magnetic field data corrected for the propagation time to the Moon were used in this study to understand the IMF condition at the Moon. The separation between ACE and the Moon was ~180 R_E during the observations, where R_E is the Earth radius (6378 km). Considering the velocity of the solar wind of 310 to 340 km/s as observed by SWIM, the solar wind propagation between ACE and the Moon was 56 to 61 min. Hence, we have assumed that the time difference from ACE to the Moon was 1 h. Figure 4 shows the IMF data observed by ACE in the GSE coordinate system. The difference between the GSE and the LSE frame is small enough (~0.18°) to consider them identical. The ACE data obtained between 1200 and 1800 UT (Figure 4, lower axis) were shifted to 1300–1900 UT at the Moon (upper axis). The magnitude of the IMF was stable at 3–4 nT over the period of interest. The magnetic field vector elevation angle, $\sin^{-1}(Bz/B)$, was almost 0, which means that the magnetic field vector was closely confined to the x_{LSE}-y_{LSE} plane during the observations. The azimuthal angle, $\tan^{-1}(By/Bx)$, was 135° before 1300 UT (~1400 UT at the Moon) following the Parker spiral. Between 1300 and 1400 UT (1400 and 1500 UT at Moon), a slightly fluctuating IMF azimuthal angle was observed. Afterward, the angle changed to 90°, meaning that the IMF direction was almost perpendicular to the solar wind velocity during the time the proton population (E) was observed.

4. Discussion

[15] The IMF configuration and the change of its direction can consistently explain the characteristics of the accelerated protons (D). Because the direction of the convective electric field ($-\boldsymbol{v} \times \boldsymbol{B}$) points toward the Northern Hemisphere throughout the observations, it is natural that the accelerated protons (D) are detected only in the Northern Hemisphere (Figure 2). The convective electric field is $\boldsymbol{E} = -\boldsymbol{v} \times \boldsymbol{B}$ = ~300 km/s × 3 nT × cos 45° = ~0.6 mV/m = ~1.1 kV/R_M, where R_M is the lunar radius (1738 km). The estimated energy is consistent with the observed energy of the accelerated protons. The change in the IMF direction at 1500 UT at the Moon can explain the disappearance of the proton flux (D) on the second orbit. For the first orbit,the azimuthal angle of the magnetic field ($\tan^{-1}(By/Bx)$) was ~135° to the Sun-Moon line. This angle means that the magnetic field direction was almost in the same plane as the orbital plane of Chandrayaan-1 (Figure 5). The backscattered protons are accelerated by the electric field and then start gyrating around the magnetic field [*Holmström et al.*, 2010]. This $\boldsymbol{E} \times \boldsymbol{B}$-drift motion is confined in the plane perpendicular to the IMF and the orbital plane in this case. Because the SWIM FoVs are perpendicular to the orbital plane, the ion gyration plane is favorable for observation by SWIM. After the magnetic field direction changed to 90° prior to the second orbit, the $\boldsymbol{E} \times \boldsymbol{B}$-drift motion was confined in the x-z plane. Because the ambient convection electric field accelerates protons in the $+z$ direction quickly, the z component of the velocity vector of the gyrating proton dominates over its x component. Such particles cannot be observed by SWIM because they do not enter the SWIM FoV, which is oblique to the motion of these particles.

[16] The ion flux on the nightside (E) is not simple to interpret. As mentioned in section 1, there were nightside ion observations by the Apollo lander reported by *Freeman* [1972], however, more detailed investigations could not be conducted because of the uncertainty of the upstream solar wind conditions. Wind [*Ogilvie et al.*, 1996; *Mall et al.*, 1998] and Nozomi [*Futaana et al.*, 2003] reported lunar-related ions, but these observations were not conducted in the near-lunar wake.

[17] Recently, the analysis of the Kaguya data obtained at a height of 100 km identified two mechanisms of the intrusion of protons into the near-lunar wake. The first

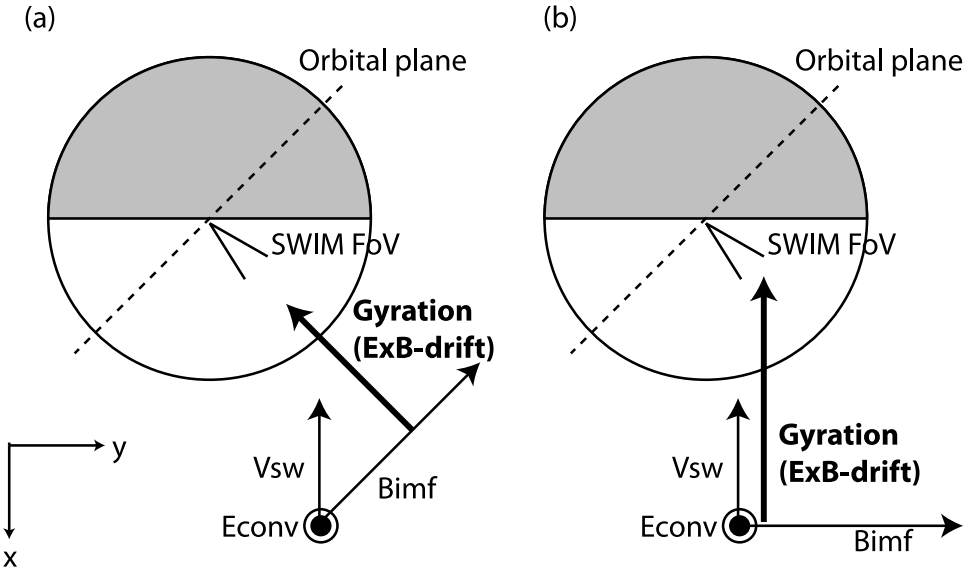

Figure 5. Illustration of the proton transport by gyromotion under the two different upstream magnetic field directions: (a) 135° and (b) 90°. The illustration is seen from the north pole (i.e., projection to the *x*-*y* plane). The SWIM field of view (FoV) is drawn at the north pole for simplicity. At the north pole the acceptance is only 10° under the nadir pointing. In Figure 5a, if the IMF direction is 135°, the IMF is almost in the same plane as the orbital plane of the observation. Therefore, the $\boldsymbol{E} \times \boldsymbol{B}$ drift is perpendicular to the orbital plane, and the SWIM may be able to see the gyrated protons. In Figure 5b, conversely, when the IMF direction becomes 90°, the gyration is only in the *x*-*z* plane; therefore, the SWIM cannot detect the gyrated protons.

mechanism is the acceleration of solar wind protons into the lunar wake by an electric potential at the wake boundary [*Nishino et al.*, 2009a]. The intrusion takes place at the wake boundary region, where the solar wind velocity vector is perpendicular to the IMF, with an asymmetry depending on the Larmor motion of the solar wind protons affected by the large inward electric field (~400 V). The second mechanism is transport of the backscattered protons from the dayside by the $\boldsymbol{E} \times \boldsymbol{B}$ drift [*Nishino et al.*, 2009b]. This intrusion can be realized when the gyroradius of backscattered protons is of the same order as the lunar radius. Indeed, the gyroradii of protons is ~1.4×10^3 km for zero initial velocity under a solar wind velocity of 400 km/s and a magnetic field of 3 nT.

[18] However, these theories cannot be applied to explain the nightside ion flux observed by the SWIM, which was propagating along the magnetic field. Figure 6 shows the observed velocity distribution functions for the solar wind sliced in the ecliptic plane (Figure 6a) and along the direction perpendicular to the ecliptic plane (v_z) (Figure 6b). In Figure 6a the fan-shaped, filled, pseudo-color image shows the phase space density of ions observed on the nightside (1454–1500 UT), and the contour lines are the solar wind protons and α particles (1357–1403 UT). The magnetic field in the solar wind reference frame estimated from the ACE data is also superimposed on the plot (Figure 6a). The cross indicates the solar wind velocity vector from the Wind/SWE data. The relatively high *y*-component velocity of the solar wind in the SWIM data is probably from instrument effects. The channels where the main solar wind component are expected, in general, have a lower efficiency than in the ground calibration. The reasons for this are yet unknown. There are no such problems in the channels where the nightside flux was observed. It is clear from Figure 6a that the observed flux is along the direction of the IMF, which is different from the Kaguya measurements. The theories to explain the Kaguya measurements thus do not apply. Additionally, note that Figure 6b shows that we can measure the 3D velocity distribution function with the assistance of the spacecraft motion and the nadir pointing.

[19] A very simple 1D model, which is based on the classical theory of a plasma expansion into vacuum along the magnetic field line, has been employed to explain the plasma distribution in the lunar wake using an analytical formulation [*Ogilvie et al.*, 1996; *Halekas et al.*, 2005]. Even though such a 1D model is too simple for detailed discussions on the physics in the lunar wake, we use this model to explain the origin of the observed nightside protons (E). Because the solar wind plasma (both protons and electrons) has a higher mobility in the direction parallel to the magnetic field line than in the perpendicular directions, the solar wind plasma past the terminator immediately starts filling the lunar wake. In the solar wind rest reference frame, the theory of 1D expansion into vacuum can be applied to the expansion into the lunar wake. The configuration of the IMF direction perpendicular to the solar wind velocity vector on 25 January 2009 is favorable for application of the 1D expansion theory. Because the pressure gradient is parallel to the magnetic field direction, the diamagnetic current ($-\nabla p \times \mathbf{B}$) can be neglected.

[20] The gyromotion in the direction perpendicular to the magnetic field arising from the thermal speed may play a

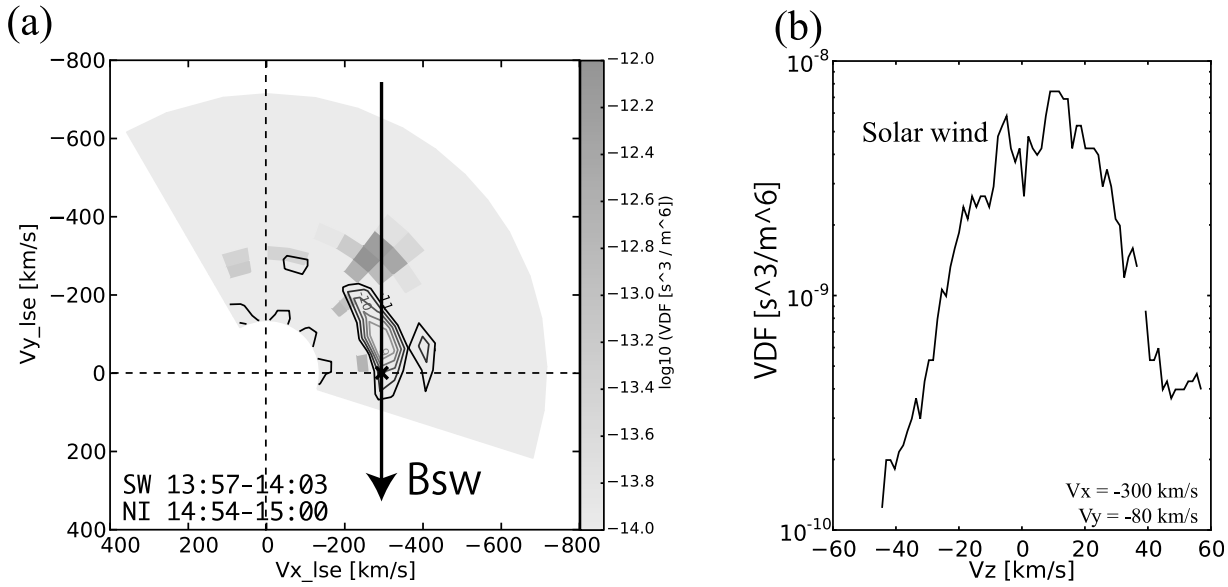

Figure 6. (a) Velocity distribution functions of the solar wind (contour lines) and the nightside ions (filled polygons) in the lunar ecliptic plane. Velocity distribution functions of solar wind ions and nightside ions are the average of the observations between 1357 and 1403 UT and between 1454 and 1500 UT, respectively. During this period the FoV of the SWIM is in the ecliptic plane. The velocity of the solar wind from Wind/Solar Wind Experiment (SWE) data is shown by the cross. The magnetic field line is superimposed in the solar wind reference frame. (b) The solar wind velocity distribution as a function of V_z. The V_z component can be measured with the assistance of the spacecraft motion and its nadir pointing. Data were taken between 1355 and 1405 UT.

role because the gyroradius is ~100 km (for protons assuming a thermal velocity of 30 km and a magnetic field strength of 3 nT), which is comparable to the spacecraft altitude. However, the gyromotion is less significant compared to the parallel expansion, and we can still apply the 1D approximation to this event. The reason is because the gyroperiod (~22 s) is long enough compared to the travel time of ~3 s for the nightside protons from the terminator to the observation point, and thus the protons experience only a part of the gyration until they are observed and the trajectory of the protons in the Moon frame does not change significantly.

[21] The 1D formulation of a plasma expansion into a vacuum is summarized by *Samir et al.* [1983]. The following assumptions are made: (a) the electrons are always in equilibrium with the electrostatic potential employed by Boltzmann's relations [e.g., *Crow et al.*, 1975]; (b) the solar wind electrons follow the Maxwell distribution functions with a constant temperature T_e over the system; (c) the ion temperature T_i is 0; and (d) there is charge neutrality. These four assumptions are rather realistic, but the problematic assumptions that have been introduced for the study of the plasma expansion into the lunar wake are as follows: (e) we neglect the surface potential, and (f) we ignore surface absorption. The latter two assumptions are quite difficult to include in analytical models, and therefore, they have been assumed by many authors explicitly or implicitly.

[22] The plasma parameters, the ion density (n_i), ion velocity (v_i), and electric potential (V), can be described as a function of the distance from the vacuum boundary at the initial state s. The set of equations can be formulated as

$$n_i = n_e = n_0 \exp\left(-\frac{s}{V_{\rm ia}t} - 1\right), \tag{1}$$

$$v = \frac{s}{t} + V_{\rm ia}, \tag{2}$$

$$V = -\frac{kT_e}{e}\left(\frac{s}{V_{\rm ia}t} + 1\right) \tag{3}$$

where t is time, n_0 is the undisturbed plasma density, n_e is the electron density, e is the elementary charge, M is the mass of the proton, and k is the Boltzmann constant. $V_{\rm ia} = (kT_e/M)^{1/2}$ is the ion acoustic velocity under assumption (c), $T_i = 0$. Wind [*Ogilvie et al.*, 1996] and Lunar Prospector [*Halekas et al.*, 2005] observations can be better explained by assuming that the solar wind electron velocity distribution has a κ distribution than by assuming a Maxwell distribution. In particular, Lunar Prospector observations are conducted at an altitude similar to that of our observation, and the electron distributions are consistent with a model using a κ distribution [*Halekas et al.*, 2005]. Therefore, comparison with a κ distribution is also worthwhile to understand the ion dynamics in the lunar wake.

[23] Table 1 reports the results of the calculated density and velocity at the spacecraft position. The SARA observations show a 2 to 3 times higher velocity than the

Table 1. Summary of the Calculation[a]

	Velocity	Density (ratio)
SARA observation	300–400 km/s	0.05%–0.2%
Modeled by Maxwellian electrons [*Samir et al.*, 1983]: T_e = 141,000 ± 38,000 K[b]	161–170 km/s	0.4%–1.2%
Modeled by κ distribution [*Halekas et al.*, 2005]: T_e = 141,000 K,[b] κ = 4.5[c]	185 km/s	0.9%

[a]SARA, Sub-keV Atom Reflection Analyzer.
[b]Taken from *Newbury et al.* [1998].
[c]Taken from *Halekas et al.* [2005].

model calculations. The observed density is lower than the model calculations by a factor of 2 to 25. However, the density ratio calculated by the 1D models depends quite sensitively on the solar wind electron temperature, which we do not know for this observation. In addition, the density calculation from the electrostatic analyzer data is not straightforward. Therefore, we can only say that there is a possibility that the observed density ratio is lower than that given by the models. In contrast, the velocity measurement by the electrostatic analyzer is more reliable, and the dependence on the models is quite small. Therefore, we can conclude that the observed velocity is significantly different from the model. This conclusion may contradict the results of the electron distribution by the Lunar Prospector [*Halekas et al.*, 2005]. The contradiction between the electron distribution, which is consistent with the 1D model, and the observed velocity of the protons, which is higher than the same 1D model, is still an open question, but it should be investigated in future.

[24] The reason for the higher velocity (2 to 3 times) of the observed protons is also an open question. One possible reason is that the 1D model is too simple to reproduce the lunar wake plasma physics quantitatively. Ion absorption by the lunar surface, which was neglected in the models, may potentially explain the higher velocity (and possibly also the lower density) of the nightside ions. As soon as the solar wind electrons or ions are absorbed by the surface, the self-similar solutions cannot be used anymore. The theoretical estimate from equation (1) is that e^{-1} (~36%) of the solar wind ions are absorbed by the lunar surface (see Appendix A). This high absorption rate may explain the possible lower proton density in the observations. In addition, the extra acceleration may be explained by the selection effect: only protons with a high-velocity component along the magnetic field can reach the observation point.

[25] The surface potential at the terminator region may also play a role [*Kimura and Nakagawa*, 2008], particularly if one considers the plasma absorption at the lunar surface. Owing to the high speed of the electrons, the solar wind electrons are absorbed by the lunar surface at the terminator and at the nightside hemisphere of the Moon. Because of the low conductivity of the lunar regolith, the absorbed electrons are "attached" at the lunar surface, generating the negative surface potential until the equilibrium of the influx of solar wind electrons and protons is satisfied.

[26] *Kimura and Nakagawa* [2008] conducted a 2D particle simulation to investigate the effect of the surface potential at the terminator. They claim that at the terminator, the electric potential becomes 60–80 V negative owing to the electron attachment to the lunar surface. The potential drop may help accelerate the protons into the wake as observed by the SWIM. When they removed the surface charging effect from their model, the acceleration of the ions decreased less at 6.5 R_L. The effect of the negative electric potential in the terminator region caused by electron attachment may also contribute to the accelerated proton signatures observed by the SWIM. However, note that *Kimura and Nakagawa* [2008] used an unrealistically large Debye length (at most $R_L/8$), and therefore, direct comparison with the data from SARA (100 km altitude) is quite difficult. A detailed comparison with simulation results using more realistic parameters is needed to understand the ion dynamics in the wake close to the Moon.

5. Summary

[27] We analyzed data from the ion spectrometer SWIM on board the Chandrayaan-1 spacecraft on 25 January 2009. During the observations the IMF conditions were stable and the geometry of the upstream electromagnetic field was relatively simple.

[28] Three ion populations in addition to the nominal solar wind ions (both protons and α particles) are identified in the SWIM data. On the dayside, backscattered protons and accelerated backscattered protons are observed, and they are similar to the populations observed earlier by Kaguya [*Saito et al.*, 2008]. These observations can be explained by single-particle motions in the IMF and the convective electric field.

[29] We also detected proton fluxes in the lunar wake region. The observed position was ~50° from the terminator inside the near-lunar wake at a height of 100 km. The flux propagates along the magnetic field in the solar wind frame; therefore, the gyromotion, IMF, and convective electric field cannot play a role. The proton energy was ~700 eV, which is slightly higher than the solar wind bulk energy of ~550 eV during the observation period.

[30] The prediction of the 1D models could not explain the velocity of the observed protons, as it was 2 to 3 times higher than the velocity given by the model. The observed velocity is higher than the prediction by the models. The reason for the difference in the velocity is still an open question, but the surface absorption effect, which is neglected in the analytical models, and the negative surface potential of the Moon at the terminator region and the nightside surface are one possible reason. The absorption of the plasma particles and the resulting large electric potential at the lunar surface could be significant for understanding the kinetics of solar wind ions in the low-altitude wake of the Moon.

Appendix A: Absorption Ratio of Protons at the Lunar Surface

[31] Here we calculate the absorption ratio of solar wind protons at the lunar surface close to the terminator. The coordinate system used here is shown in Figure A1. When solar wind protons expand into the lunar wake, a rarefaction wave is formed. The rarefaction wave front,

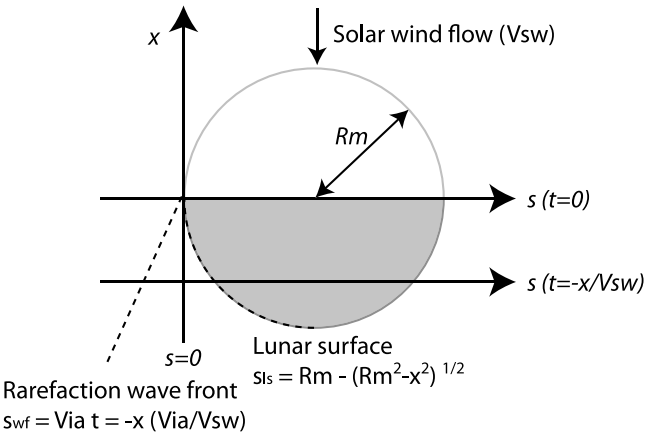

Figure A1. Coordinate system used for calculation of the absorption rate. The x axis is the Moon-Sun line identical to the LSE frame. The s axis is perpendicular to the x axis along the magnetic field, but its origin is the wake boundary at the terminator. The rarefaction wave front and the lunar surface are shown by dashed lines.

$s_{\rm wf}$, is the boundary separating the undisturbed from the disturbed solar wind. From equation (1) we know that the wave front propagates with the velocity of the ion acoustic speed:

$$s_{\rm wf} = -V_{\rm ia}t. \tag{A1}$$

The total amount of solar wind plasma that is affected by the vacuum expansion, N_t, is an integration of the density as

$$N_{\rm t} = \int_{s_{\rm wf}}^{\infty} n_i {\rm d}s = n_0 V_{\rm ia} t. \tag{A2}$$

Conversely, the location of the lunar surface, $s_{\rm ls}$, is purely geometric and can be described as

$$s_{\rm ls} = R_M - \sqrt{R_M^2 - x^2} = R_M - \sqrt{R_M^2 - (v_{\rm sw}t)^2}. \tag{A3}$$

The plasma that passes through the lunar surface (in reality, the plasma is absorbed), N_a, is again an integration of the density as follows:

$$N_a = \int_{s_{\rm ls}}^{\infty} n_i {\rm d}s. \tag{A4}$$

Substituting equations (3) and (A3) into equation (A4), the absorbed plasma density is obtained as

$$N_a = n_0 V_{\rm ia} t \exp\left(-\frac{s_{\rm ls}}{V_{\rm ia}t} - 1\right). \tag{A5}$$

The absorption rate of the solar wind protons at the lunar surface can be calculated as N_a/N_t. This formulation is only valid just after the vacuum expansion starts because the surface absorption violates the self-similar solution of equation (1). Therefore, one must take the limit of the time t to 0, which results in $N_a/N_t \rightarrow e^{-1}$ $(t \rightarrow 0)$.

[32] **Acknowledgments.** We thank the ACE MAG instrument team and the ACE Science Center for providing the ACE data. We also thank the Wind/SWE instrument team for provision of the solar wind velocity and the density data. The efforts at the Swedish Institute of Space Physics were supported in part by the European Space Agency (ESA). The effort at the University of Bern was supported in part by the ESA and by the Swiss Science Foundation. The efforts at the Space Physics Laboratory, Vikram Sarabhai Space Center, were supported by the Indian Space Research Organization.

[33] Masaki Fujimoto thanks Jasper Halekas and another reviewer for their assistance in evaluating the paper.

References

Barabash, S., et al. (2009), Investigation of the solar wind-Moon interaction on board Chandrayaan-1 mission with the SARA experiment, *Curr. Sci.*, *96*(4), 526–532.

Bhardwaj, A., S. Barabash, Y. Futaana, Y. Kazama, K. Asamura, D. McCann, R. Sridharan, M. Holmström, P. Wurz, and R. Lundin (2005), Low energy neutral atom imaging on the Moon with the SARA instrument aboard Chandrayaan-1 mission, *J. Earth Syst. Sci.*, *114*(6), 749–760, doi:10.1007/BF02715960.

Birch, P. C., and S. C. Chapman (2001), Particle-in-cell simulations of the lunar wake with high phase space resolution, *Geophys. Res. Lett.*, *28*(2), 219–222.

Crow, J. E., P. L. Auer, and J. E. Allen (1975), The expansion of a plasma into a vacuum, *J. Plasma Phys.*, *14*(1), 65–76.

Farrell, W. M., M. L. Kaiser, J. T. Steinberg, and S. D. Bale (1998), A simple simulation of a plasma void: Applications to wind observations of the lunar wake, *J. Geophys. Res.*, *103*(A10), 23,653–23,660.

Freeman, J. W. (1972), Energetic ion bursts on the nightside of the Moon, *J. Geophys. Res.*, *77*(1), 239–243.

Futaana, Y., S. Machida, Y. Saito, A. Matsuoka, and H. Hayakawa (2001), Counterstreaming electrons in the near vicinity of the Moon observed by plasma instruments on board Nozomi, *J. Geophys. Res.*, *106*(A9), 18,729–18,740.

Futaana, Y., S. Machida, Y. Saito, A. Matsuoka, and H. Hayakawa (2003), Moon-related nonthermal ions observed by nozomi: Species, sources, and generation mechanisms, *J. Geophys. Res.*, *108*(A1), 1025, doi:10.1029/2002JA009366.

Futaana, Y., S. Barabash, M. Holmström, and A. Bhardwaj (2006), Low energy neutral atoms imaging of the Moon, *Planet. Space Sci.*, *54*(2), 132–143.

Halekas, J. S., S. D. Bale, D. L. Mitchell, and R. P. Lin (2005), Electrons and magnetic fields in the lunar plasma wake, *J. Geophys. Res.*, *110*, A07222, doi:10.1029/2004JA010991.

Holmström, M., M. Wieser, S. Barabash, Y. Futaana, and A. Bhardwaj (2010), Dynamics of solar wind protons reflected by the Moon, *J. Geophys. Res.*, *115*, A06206, doi:10.1029/2009JA014843.

Kallio, E. (2005), Formation of the lunar wake in quasi-neutral hybrid model, *Geophys. Res. Lett.*, *32*, L06107, doi:10.1029/2004GL021989.

Kimura, S., and T. Nakagawa (2008), Electromagnetic full particle simulation of the electric field structure around the Moon and the lunar wake, *Earth Planets Space*, *60*, 591–599.

Lin, R. P., D. L. Mitchell, D. W. Curtis, K. A. Anderson, C. W. Carlson, J. McFadden, M. H. Acuna, L. L. Hood, and A. Binder (1998), Lunar surface magnetic fields and their interaction with the solar wind: Results from lunar prospector, *Science*, *281*(5382), 1480–1484.

Mall, U., E. Kirsch, K. Cierpka, B. Wilken, A. Söding, F. Neubauer, G. Gloeckler, and A. Galvin (1998), Direct observation of lunar pick-up ions near the Moon, *Geophys. Res. Lett.*, *25*(20), 3799–3802.

McCann, D., S. Barabash, H. Nilsson, and A. Bhardwaj (2007), Miniature ion mass analyzer, *Planet. Space Sci.*, *55*(9), 1190–1196.

Newbury, J. A., C. T. Russell, J. L. Phillips, and S. P. Gary (1998), Electron temperature in the ambient solar wind: Typical properties and a lower bound at 1 AU, *J. Geophys. Res.*, *103*(A5), 9553–9566.

Nishino, M. N., et al. (2009a), Pairwise energy gain-loss feature of solar wind protons in the near-Moon wake, *Geophys. Res. Lett.*, *36*, L12108, doi:10.1029/2009GL039049.

Nishino, N. M., et al. (2009b), Solar-wind proton access deep into the near-Moon wake, *Geophys. Res. Lett.*, *36*, L16103, doi:10.1029/2009GL039444.

Ogilvie, K. W., J. T. Steinberg, R. J. Fitzenreiter, C. J. Owen, A. J. Lazarus, W. M. Farrell, and R. B. Torbert (1996), Observations of the lunar plasma wake from the Wind spacecraft on December 27, 1994, *Geophys. Res. Lett.*, *23*(10), 1255–1258.

Russell, C. T., and B. R. Lichtenstein (1975), On the source of lunar limb compressions, *J. Geophys. Res.*, *80*(34), 4700–4711.

Saito, Y., et al. (2008), Solar wind proton reflection at the lunar surface: Low energy ion measurement by MAP-PACE onboard Selene (Kaguya), *Geophys. Res. Lett.*, *35*, L24205, doi:10.1029/2008GL036077.

Samir, U., K. H. Wright Jr., and N. H. Stone (1983), The expansion of a plasma into a vacuum: Basic phenomena and processes and applications to space plasma physics, *Rev. Geophys.*, *21*(7), 1631–1646.

Trávníček, P., P. Hellinger, D. Schriver, and S. D. Bale (2005), Structure of the lunar wake: Two-dimensional global hybrid simulations, *Geophys. Res. Lett.*, *31*, L06102, doi:10.1029/2004GL022243.

Wieser, M., S. Barabash, Y. Futaana, M. Holmström, A. Bhardwaj, R. Sridharan, M. B. Dhanya, A. Schaufelberger, P. Wurz, and K. Asamura (2010), First observation of a mini-magnetosphere above a lunar magnetic anomaly using energetic neutral atoms, *Geophys. Res. Lett.*, *37*, L05103, doi:10.1029/2009GL041721.

K. Asamura, Institute of Space and Astronautical Science, 3-1-1 Yoshinodai, Sagamihara, Japan.

S. Barabash, Y. Futaana, M. Holmström, and M. Wieser, Swedish Institute of Space Physics, Box 812, Kiruna SE-98128, Sweden. (futaana@irf.se)

A. Bhardwaj, M. B. Dhanya, and R. Sridharan, Space Physics Laboratory, Vikram Sarabhai Space Center, Trivandrum 695 022, India.

A. Schaufelberger and P. Wurz, Physikalisches Institut, University of Bern, Sidlerstrasse 5, CH-3012 Bern, Switzerland.